Design of a Self-Reconfigurable Drain Mapping Robot With Level-Shifting Capability

RIZUWANA PARWEEN[1], (Member, IEEE), **ABDULLAH AAMIR HAYAT**[1],
KARTHIKEYAN ELANGOVAN[1], **KOPPAKA GANESH SAI APUROOP**[1,3],
MANUEL VEGA HEREDIA[2], **AND MOHAN RAJESH ELARA**[1]

[1]Engineering Product Development, Singapore University of Technology and Design, Singapore 487372
[2]Apt of Engineering and Technology, Universidad Autónoma de Occidente, Los Mochis 81223, Mexico
[3]Nano Electronic Engineering and Design, Chang Gung University, Taoyuan City 333, Taiwan

Corresponding author: Rizuwana Parween (rizuwana_parween@sutd.edu.sg)

ABSTRACT Nature has always been an inspiration for engineers and designers to have technological inventions. The postures, locomotion and gait cycles of animals are usually smooth, dynamically stable, and highly adaptable in an unknown terrain. Based on a giraffe's leg folding pattern, we develop a quadruped hybrid drain mapping robot with modular sub-systems, four bar inversion mechanism based legs and bi-directional rolling wheel, named, Tarantula-II. The platform undergoes self-reconfiguration and achieves variable height and width, which in turn helps in navigation in a drain with multiple level-shifts. This paper describes the key features of giraffe's limb, how the folding pattern of the limbs are implemented in the robot design. In addition, we discuss the detailed mechanical design of platform, the kinematics analysis of each leg, kinematics of the platform with respect to wheels, and structural analysis of the platform under different gait condition. Applying the kinematics formulation and posture correction algorithm, we verify the mobility and level shifting capability of the platform both in lab setting and drain environment.

INDEX TERMS Drain mapping robot, self-reconfiguration, level-shifting, bi-directional rolling wheel.

I. INTRODUCTION

Drainage system has tremendous impact on the economic and social aspects of the urban community. Stagnant water and clogging due to wastes in drain usually cause mosquito breeding and unhealthy environments causing epidemic diseases. This necessitates for constant maintenance of drains by trained labor for to upkeep the hygiene of the community In addition, it is important to monitor the state of the drain wall periodically and inspection of wall and stagnant water in closed drain are challenging, hazardous, and unsafe for the human labor. Hence, in order to decrease the human involvement while drain inspection, robotic equipment designed for specific condition of drains and the operators were trained to operate these robotic equipment from outside of drain.

There are various type of drainage system including closed pipelines, side drains to carry rainwater, closed surface drains, sewerage system, etc. across the globe. The closed drain is usually carrying excess water along the channel and discharge into larger collectors drains. The channel width varies substantially 80 cm to 110 cm and is covered with a heavy metallic grate. Figure 1 (a) shows the schematic of the drain with multiple level shifts varying from 30 cm to 110 cm for a drainage system.

For a drain environment with substantial variation in width and eight, we believe that there is a need for a robust design for a self-reconfigurable robot to adapt variable width and height of the drain. In order to navigate the platform along the flat drain and cross the levels as well, a quadruped robot with hybrid systems including rolling wheels and legs would be the best fit. Its due to the fact that rolling wheels are the most appropriate modes of locomotion in both rough and flat terrain and legs are more suitable for crossing the levels and undergoing height variation.

Considering the design requirement for the robot, the state of the art for the quadruped, hybrid and drain inspection robots are highlighted. Literature reveals that the quadruped robots have been existing since the fourth century. The first design of quadruped was built in the form of a four-legged wooden walking machine. Gradually, with
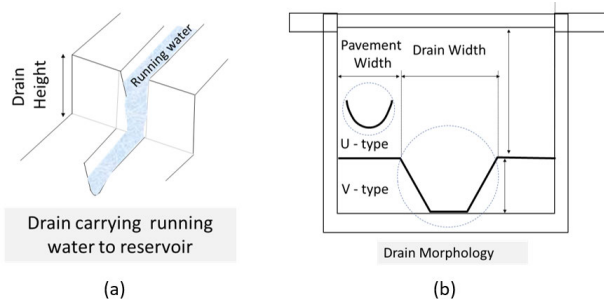
The associate editor coordinating the review of this manuscript and approving it for publication was Chenguang Yang.

FIGURE 1. (a) Schematics of a drain environment showing level-shift (b) Cross-section of drain with level-shift.

the development of powerful computing and on-board control systems, many walking machines have been built, and research moving moving forward greatly. In 1980s, the G.E. Quadruped [1] and the Phoney Poney [2] were the first to successfully realize a walking machine. The Titan series (I-IV) [3] and PV II [4], are quadruped walking machines with onboard control systems with legs inspired from insects and reptiles. Later versions of Titan series were sprawling-type quadruped robot capable of gaining high velocities and energy efficient walking [3], [5], [6]. BISAM, a four-legged walking machine, consists of a spinal column that provides better stability and also achieves reptile and mammal- inspired locomotion [7]. Yanagida *et al.*, developed a bio-inspired self-configurable robot, called Scorpio for urban search and rescue missions [8]. Campos *et al.*, developed a sprawling robotic leg inspired by the limb postures of reptilian animals and showed that the robotic leg can trace concave, convex curves, and straight lines and explained the path planning procedure [9]. Wang *et al.*, presented a bio-inspired controller for realizing the bounding gait of an SQBot, which is a quadruped robot with a spine joint [10].

Wheeled robots are robust, simple in design, fast and easy to control. Legged robots have usually better terrain adaptability than wheeled robots. Robots with hybrid locomotion were developed to exploit the terrain adaptability of legs and simpler control and high speed capability of the wheels [11]–[14]. There were bio inspired hybrid systems with mammal type leg attached to wheels as discussed below. Halme *et al.*, developed a robot with four wheeled legs and each leg has three degree of freedom with a rubber wheel attached to it [15]. Dai *et al.*, developed a robot with four legs (two in the front and two rear legs) and two wheels in the middle, for the exploration [16]. Suwannasit *et al.*, developed a leg-wheel hybrid robot, with two active two degrees of freedom legs in the front and two passive rear wheels at the rear end [17].

Drain inspection robots were developed over the years to mainly to reduce human involvement in drainage inspection and cleaning. For example, Kirkham *et al.*, developed an in-pipe semi-autonomous vehicle, PIRAT, for sewer inspections based on a quantitative technique [18]. It has automated the measurement and analysis of the internal geometry

of the sewer to detect, and classify defects using artificial intelligence techniques. There are other semi-autonomous robots KARO [19] and the Pearl Rover [20] robot for pipe and in-water inspections, respectively. KURT [21], MAKRO [22], and KANTARO [23] are the un-tethered autonomous robots, that carry all required equipment on-board, and inspect sewers and pipelines [24]. Baghani *et al.*, developed a robot, called University of Tehran-Pole Climbing Robot (UT-PCR) to climb and inspect vertical and inclined pipes, chimneys [25]. Ratanghayra *et al.*, reported a robot capable of climbing ropes at different inclinations [26]. Even though these robots perform the required tasks with hlspecial, they fail to adapt the variable drain width and multiple level changes for a drain morphology as shown in Fig. 1 (a).

The precedence of the Tarantula-II is based on the first version of the robot here referred as Tarantula-I reported in [27]. The two versions can be compared using the framework for evaluating the autonomy of the self-configurable robot as reported in [28]. The autonomy index (AI) calculated based on the six factors, namely, perception, workspace, interface autonomy, reconfiguration planning, decision making and execution levels as [1,2,0,1,0,1] resulting in AI as 1.1. While indicator parameters for Tarantula-II is improved with the improved design and sensors integration as [1,2,0,1,2,2] resulting in AI as 2.5. The objective of this platform is to move inside the drain environment and identify the locations of mosquito infestation. Tarantula-I platform has a central body called the trunk, with four legs attached to it. Each leg was having four degrees of freedom of motion via RPRR (R: revolute, P: prismatic) joints and telescopic extension mechanism. The telescopic extension was based on screw mechanism which took longer time to extend. The chain-sprocket mechanism was used for the power transmission to achieve simultaneous actuation of the two legs in the frontal plane using a single motor. However, the chain sprocket mechanism in Tarantula-I suffers from slippage which resulted in variable velocity and reduced efficiency. Another drawback observed was with the wheels that were having one-point contact with the ground resulting in an unstable platform and with it this design the level shift was not achieved successfully. To overcome the issues as mentioned above, we obtain the inspiration from the folding pattern of giraffe's leg and the associated degrees of freedom and build a new version of a self-configurable drain mapping robot called, Tarantula-II, overcoming the issues observed in the previous version.

This paper outlines the design concept, robot architecture including mechanical design, electronics layout, and software architecture of the platform, kinematics formulations of the robot platform, simulation and experimental results during static posture, respectively.

II. DESIGN INSPIRATION AND SYSTEM REQUIREMENTS
Giraffes are the tallest land animals with long legs. The hind legs are relatively shorter than the front legs. Each hind leg comprises two slender bones, connected with
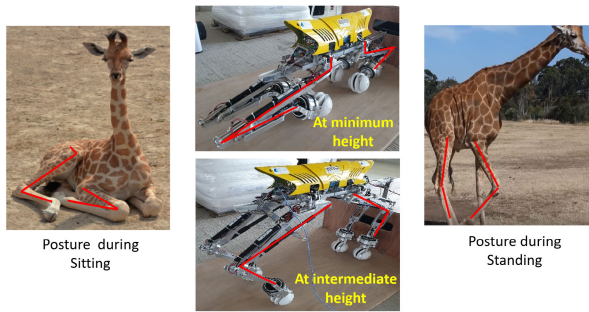
FIGURE 2. Sitting and standing postures of a giraffe [29], including and equivalent bio-inspired postures of Tarantula-II.

FIGURE 3. Tarantula-II, the drain mapping robot platform.

FIGURE 4. CAD model showing the leg, wheel and abduction mechanism of the Tarantula-II Platform.

ligaments which are made up of elastic elements (collagen and elastin) [30]. These elements act as spring that store energy to hold the giraffe's body up and support the body weight. Figure 2 shows the angular positions of the limbs of each leg during different postures of a giraffe. We obtain the following underlying design inspiration from giraffe's leg anatomy.

- The hind leg has a unique mechanism that makes the animal lie down on the ground with its body on top of its folded hind legs. Each hind leg can bend forward about the femur-tibia joint and splay to side about the hip joint. It implies that the hind leg has three degrees of freedom with mobility in two orthogonal planes.
- During sitting position, the fore legs are bent with the lower limb towards the posterior end, the hind legs are bent with the lower limb towards the anterior end. Hence, both fore and hind legs maintain a unique posture, called outward folding, during sitting as shown in Fig. 2.

With the help of the degree of freedom associated with each limb and the outward folding pattern of both fore and hind legs, the animal is able to accommodate the large body weight with stable postures during sitting and standing. With the outward folding capability of both limbs, the body's center of mass is always lie in the plane containing the contact points of the foot and ability to hold large body weight. Using these concepts, we build a hybrid quadruped drain mapping robot called, Tarantula-II, with bio-inspired postures as shown in Fig. 2. Figure 3 shows the platform with different parts. This platform achieves height variation using two linear actuators that effectively rotate the linkages. This limitation was overcome with the modified design of the wheels with the bidirectional rolling wheel and modified the power transmission mechanism by replacing the chain sprocket with two spur gears with an idler in between. The platform is designed to meet the following objectives:

- The platform should have the ability to move inside the drain environment holonomically with greater stability.
- The trunk or body of the platform should be parallel to the ground to achieve the stable posture, and is also
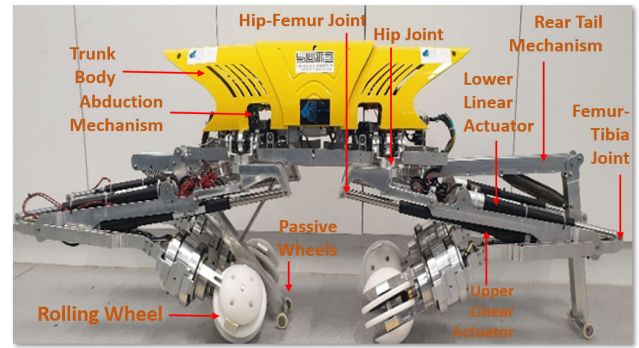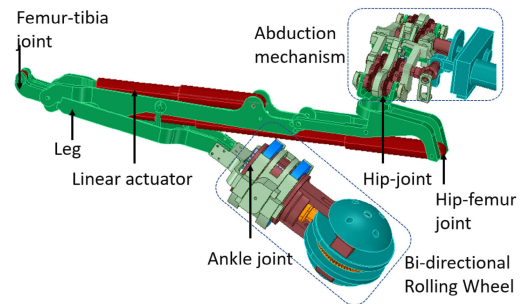
helpful in mapping the drains with two dimensional LiDAR.
- The platform should perform the level shift of upto a meter height for the drainage system shown in Fig. 1.
- The platform should have multiple stable configurations.

III. STRUCTURAL DESIGN OF THE PLATFORM

The entire Tarantula-II is a quadruped hybrid locomotion platform has three sub-mechanisms, namely abduction, leg, and wheel mechanisms, as shown in Fig. 4. The trunk is the primary supporting structure of the platform and is design to be placed parallel to the drain section. The trunk cover is made of high-grade plastics to reduce the weight. All the structural components of abduction unit, legs, and wheel holders are made of Aluminium material. The trunk accommodates a suspension mechanism that used to support the electronics module and an abduction mechanism. The leg mechanism is designed based on the giraffe's hind leg. Each leg has three parts, the hip, femur, and tibia, shown in Fig 4. The hip module is connected to the trunk with a revolute joint (called hip joint), that provide abduction movement to the entire leg. Each femur module consists of two linear actuators, with two revolute joints at the proximal end (hip-femur) and proximal ends. The revolute joint at the proximal end of a linear actuator connects the femur with the hip, called a hip-femur joint. The revolute joint at the distal (femur-tibia) end of the linear actuator connects the femur with the
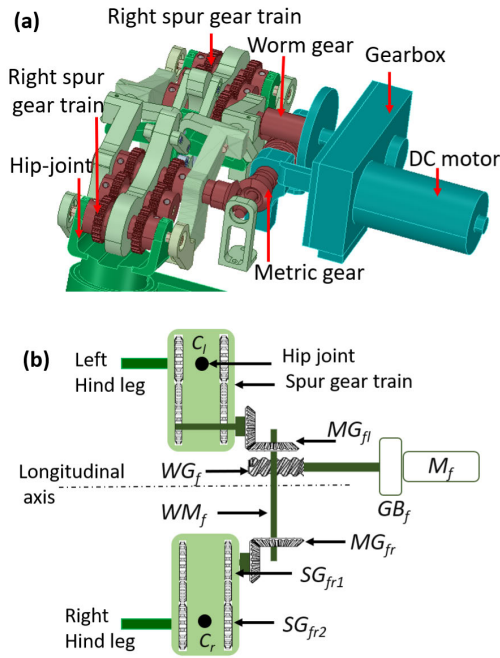
FIGURE 5. (a) CAD model and (b) Schematic layout of the posterior side of the simultaneous abduction mechanism.

FIGURE 6. CAD model of the wheel mechanism showing the different parts.

tibia, called femur-tibia joint. The other end of the tibia is connected to the steering mechanism of the omnidirectional wheel, called ankle joint.

1) SIMULTANEOUS ABDUCTION MECHANISM
The platform consists of two abduction mechanisms at the anterior and posterior ends of the trunk. It is designed to reconfigure its leg position during deployment. The anterior abduction mechanism provides zero to 180 degrees of rotation of both (left and right) fore legs in the frontal plane of the platform at the same time instant. The posterior abduction mechanism also rotates both hind legs simultaneously in the frontal plane. During reconfiguration, both abduction mechanisms synchronously rotate both fore legs and hind legs and maintain fixed wheel spacing. Figure 5 shows the schematic diagram of the anterior and posterior abduction mechanisms and the detailed working principle of the anterior abduction mechanism is described.

The anterior abduction mechanism is driven by a DC motor (M_f) connected to a mechanical gearbox (GB_f) with a gear ratio of n_1 placed along the longitudinal axis, shown in Fig. 5 (b). The motor shaft is connected to a worm gear (WG_f) and a worm (WM_f). The ends of the worm shaft are further attached to two metric gear sets, i.e., MG_{fr} and MG_{fl}. The bevel shafts of each gear set are orthogonal to each other. The driven bevel gear is connected to two sets of the compound spur gear train, i.e., SG_{fr1} and SG_{fr2} with a small spacing. At the location C, the distal end of this spacing, the trunk is connected to the leg by a revolute joint with an axis parallel to the longitudinal axis. This hip joint actuates the left foreleg from 0 to 180 degrees in the frontal plane.
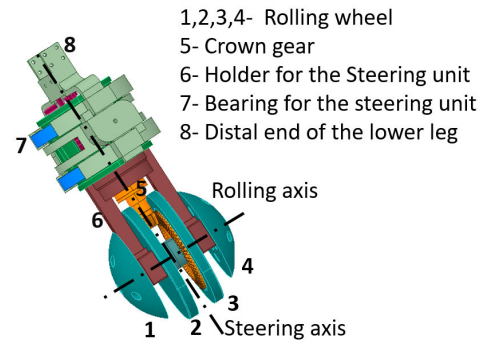
The abduction mechanism is supported by a suspension system consisting of a damper that supports electronics components and the trunk subsystems absorb and dampens shock [27]. The angular speed of the hip joint is a function of the rotational speed of the driving motor and the speed ratios of the gears, as given by Equation 1.

$$\omega_1 = \frac{\omega_0}{g_1 g_2 g_3 g_4} \tag{1}$$

where, g_1 = The speed ratio of the gearbox attached to the driving motor

g_2 = Speed ratio of the worm gear

g_3 = Speed ratio of the bevel gear

g_4 = Speed reduction of the compound gear train

ω_0 = Input angular speed of the DC motor

$\omega_1 = \dot{\theta}_1$ = Angular speed of the entire leg about its hip joint attached to the trunk during abduction.

2) ROLLING WHEEL MECHANISM
Figure 6 shows the CAD model of the rolling wheel mechanism. This wheel mechanism has two degrees of freedom including steering and rolling and provides bidirectional rotation to the wheel. By synchronizing the movement of each leg, the platform can achieve holonomic locomotion. The wheel assembly consists of rolling and steering wheel units, and each unit is driven independently. There are two DC motors, i.e., M_r and M_s (12 Volt and 80 rpm) present inside the mechanism.

The rolling wheel unit is a modular wheel consists of four distinct parts with equal spacing in between. Their parts are made up of Delrin material that provides sufficient strength during locomotion. The rolling unit is mounted on a single wheel shaft (S_r) with a crown gear mechanism. The gear shaft connects the motor M_r that drives the four parts of the wheel. Rotation of the rolling wheel unit about rolling axis provides forward and backward locomotion.

The steering unit consists of wheel plates and plate holder. The wheel plates, made up of Aluminum, are placed inside spacing of the rolling wheels. The distal end of the wheel plates is attached to a M_s motor via a spur gear mechanism. The motor M_s motor rotates the wheel and the holder about

the steering axis and provides side wise locomotion. The spur gear mechanism is supported by two bearing, i.e., outer and inner bearing. The outer bearing holds the distal end of the leg through the main holder.

A. ELECTRONICS AND CONTROL MODULE

Tarantula-II utilizes the mechanical aspects of the vehicle and the steering model to actuate the locomotion. A microcontroller namely Arduino is employed to achieve control over the actuators and the motors that are responsible for the locomotion and reconfiguration. The microcontroller is safely secured inside the trunk of the robot. A single-board computer (SBC) namely Raspberry Pi model B is also secured inside the trunk to which the aforementioned microcontroller is connected. The SBC runs the ROS framework, here it runs the ROS Kinetic version, and is termed as the slave PC. The communication to the microcontroller is established over the USB. The intended functions of the microcontroller are to receive the command from the SBC and trigger the corresponding motor drivers and to transmit the motor feedback to the SBC. With the presence of numerous motors for various operations, a cluster of motor drivers is used. The current motor drivers used are supplied by RoboClaw which has a capable output of 7A with an input of 24V. Each motor driver has a unique hexadecimal address and can be connected and accessed by utilizing the CAN communication protocol. The microcontroller will act as the master node to transmit and receive the control and the feedback from the motors connected over the CAN network. There are a pair of motors in each wheel and a pair of linear actuators in each leg and this makes the total count of eight motors in all the wheels and 8 linear actuators on all the legs. The linear actuators are custom made to fit our requirements whereas the motors are supplied by RoboClaw. Currently, the robot utilizes the tethered DC power supply where the cluster of the motor drivers is set to run at 24V. The current version of the robot does not employ any of the sensors apart from the aforementioned sensors. Efforts are being made to employ intelligent sensors such as laser range finder for an effective mapping of the drainage, proximity and infrared sensors to detect the level changes.

It is certitude that a well-defined software architecture has to be developed so as to display stable electromechanical abilities of the robot. The platform is developed on the existing ROS framework with custom added plugins and python modules. The system architecture can be assimilated starting with the master PC, shown in Fig 7. The master PC is the control station where a user is given access to the Graphical User Interface (GUI) specially designed to control the robot. On the master PC, there is a master ROS running which oversees all the basic processes related to the software startup of the robot. The ROS version used is ROS Kinetic. Under the master ROS, the GUI houses the controls of all the motors and electronics onboard. The GUI is a ROS user interface plugin which has the ability to issue various custom ROS commands to the slave PC. A slave PC is secured on the robot, which
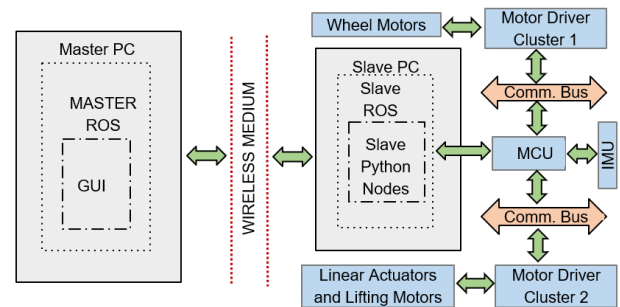

FIGURE 7. Communication system and electronics system layout of Tarantula-II.

also runs a slave ROS system. The slave ROS is patched to the master ROS on the master PC, i.e. the slave ROS shares the roscore that is running on the master PC. By sharing one roscore, the topics and messages can be shared between two computers.

A microcontroller unit (MCU) is connected to the slave PC. The slave system has three set of components responsible for the synchronized movement of the robot. The first component is a set of motors responsible for the locomotion of the robot. The second component is a set of linear actuators that are secured on the legs of the robot and are responsible for the motion of the robot vertically. The third component is a pair of high torque motors which are responsible for the lateral movement of the legs. All three set of components are connected to the MCU, obeying the commands issued by the slave PC. All the motors and linear actuators are driven by a cluster of motor drivers which communicate over CAN communication. The MCU supervises this communication bus. Since the robot can move vertically increasing and decreasing the height, there is an auxiliary ROS node which oversees the stability of the robot if it is on uneven surfaces.

An IMU sensor is connected to the MCU, and the IMU data is monitored by the ROS node which oversees the stability of the robot during the vertical motion during level-shift, shown in Fig. 8.

IV. STRUCTURAL ANALYSIS

The structural analysis of platform plays an important role in the process of designing the components and subsystems. For Tarantula-II platform, the gear train mechanism, the abduction mechanism, and leg as these are the critical components to analyze. This section outlines the simulation results of these subsystem. During analysis, the 3-D model of the platform was imported to the Fusion 360 environment and then material properties, boundary details and loading condition were applied.

A. LEG MECHANISM

The leg of the Tarantula-II platform has two different gait conditions, i.e., stance during locomotion and swing phase during level-shifting. During level-shifting, all the legs are in extended state, and the platform attains its maximum height. During level shifting, the platform undergoes three different
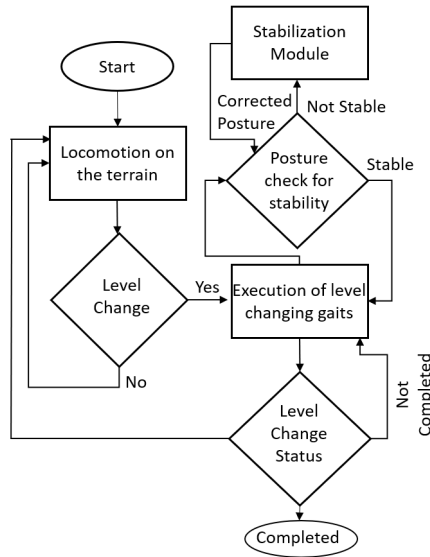
FIGURE 8. Stability algorithm of the platform during level shifting.

FIGURE 9. Mode shapes of the platform with extended legs in contact with ground.

FIGURE 10. Mode shapes of the platform with three legs in contact with ground.

FIGURE 11. Mode shapes of the platform with two legs in contact with ground.

FIGURE 12. Mode shapes of the platform with retracted legs.

type of boundary contacts, i.e., one leg in swing phase, two legs are in swing phase, all the four wheels are in contact with the ground. However, during locomotion, all the legs are in retracted length, and the platform moves in its lowest height. It either supports the body load during stance phase or sustain its own load during swing phase of level shifting, when the leg is in not in contact. Hence, we carried out both modal and static analysis to check the vibration, stress and deformation pattern of the leg for different gait conditions. Figure 9-12 show the mode shape of the platform with extended legs and retracted legs with above mentioned boundary condition. The first natural frequency of the platform with retracted legs (25.3 Hz) are higher than the platform with extended legs with different boundary conditions. It implies, during level shifting, the abduction motor and linear actuators, and the wheel motors are required to be operated below the natural frequency of the platform with two swinging legs (5.3 Hz), i.e., 300 rpm.

The deformation and stress pattern of the platform with extended legs were estimated by carrying static structural analysis for the same boundary details. Figure 13-16 show the deformation and stress pattern for different boundary setting and leg length conditions. For all the cases, the deformation of the platform is found to be less than 2.5 mm, which is less than the platform height. The location of the maximum stress is found at the sharp corner due to stress concentration factors. The most of parts the platform undergoes the Von-mises stress in the range of 20 to 50 Mpa which is less the critical stress limit of the Aluminium material.

B. GEAR MECHANISM

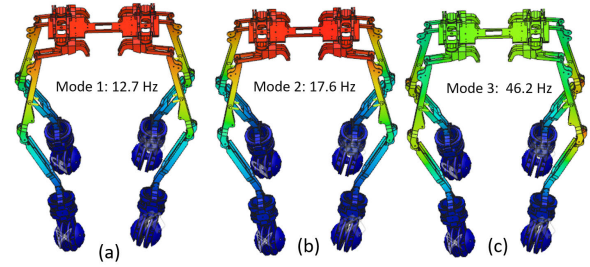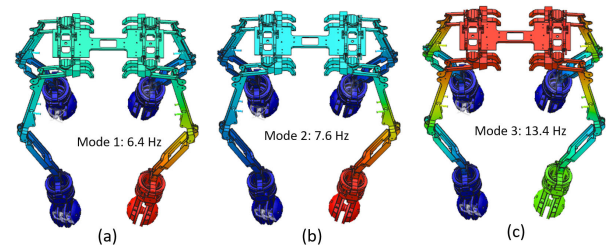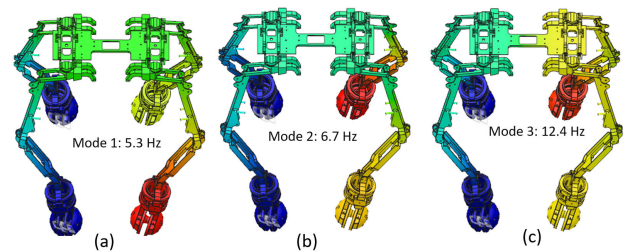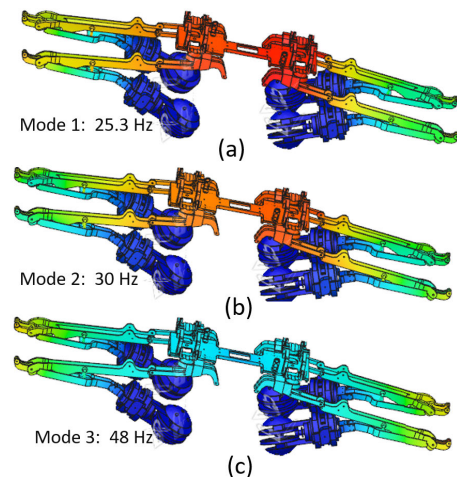In Fusion 360, the gear train model was meshed with tetrahedron elements with average element size of 1 mm. Figure 17 shows the mesh model of the gear train with of 108644 nodes and 61519 elements. The first six natural frequencies and their mode shapes were analyzed. For modal analysis, the cylindrical supports were applied as the bearing
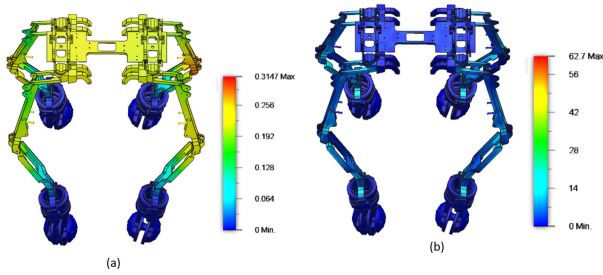
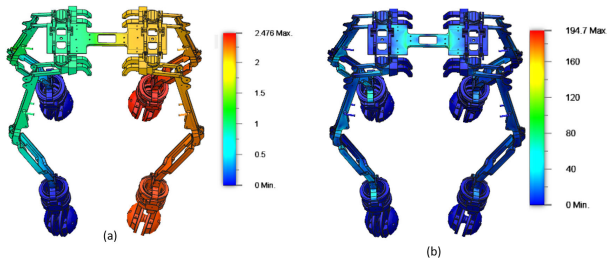**FIGURE 13.** (a) Deformation (b) Stress pattern of the platform when all legs are in contact with the ground.

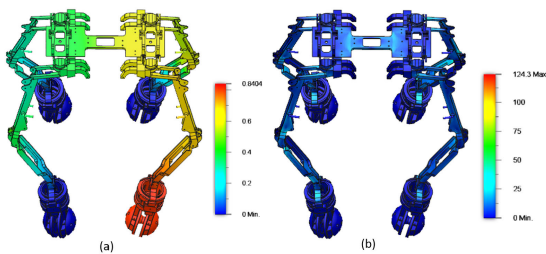**FIGURE 14.** (a) Deformation (b) Stress pattern of the platform when two rear legs are in contact with the ground.

FIGURE 15. (a) Deformation (b) Stress pattern of the platform when three legs are in contact with the ground.

FIGURE 16. (a) Deformation (b) Stress pattern of the platform for the legs are in retracted position.
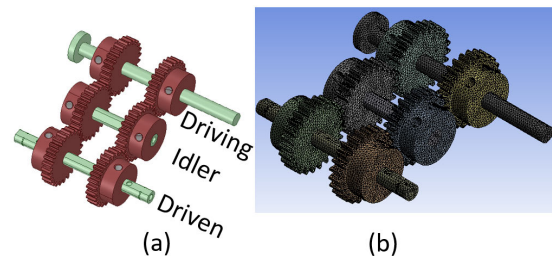
FIGURE 17. CAD and meshed model of the gear train.
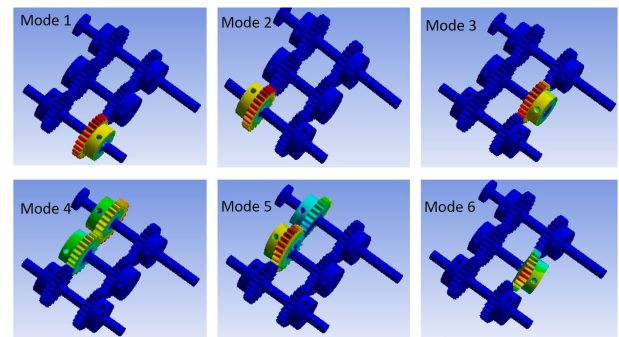
FIGURE 18. Mode shape of the gear train.

supports for the gear components, which allows rotational motion along the shaft axis but restricts axial motion and radial motion. Figure 18 shows the mode shapes of the gear train. These modal frequencies are in the kHz range, which is far greater the system's natural frequency (which is Hz).

For static analysis of the abduction mechanism, the gravitational load due to the component's weight was applied. The load bearing capability of the wheel module was tested by applying a distributed load of 200 N along the wheel axis. Figure 19(a) and (b) show the deformation pattern of the abduction mechanism and wheel respectively. The maximum deformation of the abduction unit and wheel were found to be 0.006 and 0.007 mm, which is less the critical length. The shaft is used to connect a motor to the gear train and also transfers the motor torque to actuate the hip joint gear trains. There is high chance that the shaft suffers from the cyclic loading of bending and twisting moments. This cyclic loading may lead to structural failure while locomotion and level-shifting. In order to check the load bearing capability of abduction mechanism at the hip joint during swing
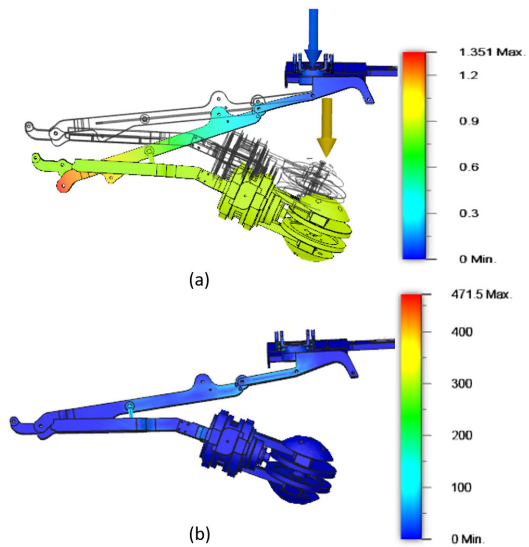
phase, static structural analysis was carried out on the shaft of the hip-joint. A load of 200 N is applied on each hip joint. Figure 19(c) shows the deformation pattern of the connecting shaft. The maximum deformation of the connecting shaft is 0.04 mm which is less than the one-tenth of the shaft diameter (8 mm). In all the above static loading cases, the maximum Von-mises stress is less than the ultimate yield strength of aluminium. Hence, the design is considered to be safe.

FIGURE 19. Deformed shape of the (a) abduction mechanism, (b) wheel module, and (c) shaft at the hinge joint carrying the lag.

a) Four axis of rotations in each leg including two orthogonal rotations in each wheel

b) Subsystems of leg mechanism

FIGURE 20. Degrees of freedom in a leg of Tarantula-II.

V. KINEMATICS OF TARANTULA-II

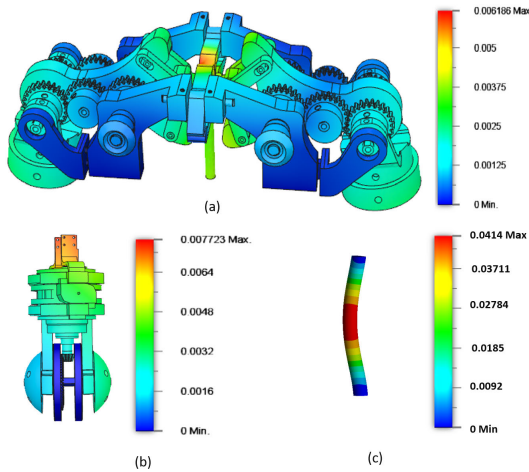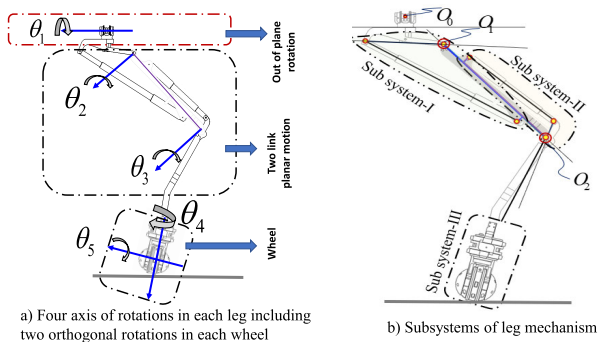In this section, the kinematic requirements for the self-reconfigurable drain mapping robot which is designed for the drain inspection task are discussed. The degrees of freedom provided to each of the four legs is described using the sub systems for its kinematic formulation. The kinematic of the spatial wheel design with omnidirectional feature which is used for the locomotion inside the drain is also explained.

A. ACTUATION OF LEG

The four degrees of freedom is provided in each leg of the Tarantula-II. Figure 20 (a) shows the four angles represented using θ_i where $i = 1, 2, 3, 4$. Note that the rotation of joint attached to the body or trunk of the Tarantula-II using the one degree of freedom hip joint. The rotation of femur and tibia are in a single plane which are denoted using θ_2 and θ_3 as shown in Fig. 20 (a). The change of height of the trunk is attained using the two link planar motion [Fig. 20 (a)]. Moreover the end-effector attached to the end of two link planar motion is the spatially designed wheel which has two independent rotations resulting in the omnidirectional locomotion of the Tarantula-II. The kinematics of a single

a) Inversion of four bar mechanism as sub-system-I
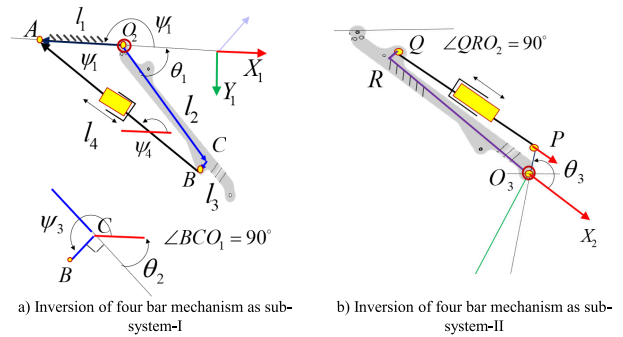
b) Inversion of four bar mechanism as sub-system-II

FIGURE 21. Four bar inversion mechanism to convert linear actuation achieve rotation in a leg of Tarantula-II.

wheel is also explained in the subsequent sub-section. The rotational motion in the form of variation in θ_1 and θ_2 are attained using the four bar inversion mechanism as shown using subsystem-I and subsystem-II in Fig. 20 (b). The vector diagram of subsystem-I, i.e., an equivalent of four bar inversion mechanism is presented in Fig. 21 (a). Note that the variation in the length of linear actuator act as an input which results in the variation of magnitude and direction of vector l_4. The variables associated with the four bar inversion mechanism is shown in Fig. 21 (a) using O_1CBA as in Fig. 20 (a) and the loop closure equation is given by:

$$l_1 = l_2 + l_3 + l_4 \qquad (2)$$

where l_i with $i = 1, 2, 3, 4$ are the vectors associated with each links of subsystem-I. The component of above equation along the axis represented using X_1Y_1 are written as:

$$l_1 \cos(\psi_1) = l_2 \cos(\theta_2) + l_3 \cos(\psi_3) + l_4 \cos(\psi_4) \quad (3)$$
$$l_1 \sin(\psi_1) = l_2 \sin(\theta_2) + l_3 \sin(\psi_3) + l_4 \sin(\psi_4) \quad (4)$$

Note that l_4 is variable which is changing with the linear actuator movement and the angle θ_2 and ψ_3 related by $\theta_1 - \psi_3 = \pi/2$. Also ψ_1 is constant and it is along the X_1-axis hence the magnitude of $\psi_1 = 180°$. The variation in length of linear actuator is related to the variation in joint rotation θ_2 is obtained by squaring and adding equation. (16) and (17) and then simplifying as:

$$l_4^2 = A + B \cos\theta_1 - C \sin\theta_1 + D \cos\theta_1 \sin\theta_1 \qquad (5)$$

where $A = l_1^2 + l_2^2 + l_3^2$, $B = -2l_1 l2$, $C = -2l_1 l_3$, $D = 4l_2 l_3$. Note that l_i are constant value defined using the assembly and its magnitude can be taken from the CAD. The magnitude of variation in linear actuator length is given by the hall-effect sensor which is attached with the linear actuators used similar to encoders for the rotary motion. Hence the variation of θ_2 and θ_3 which is a function of the change in the length of linear actuators, i.e., Length of AB and QP in Fig. 21 a and b respectively are found by solving non linear trigonometric relation given in Equation (18).

Subsystem-II has exactly the same mechanism where the variation in the angle θ_3 is controlled by the variation in the
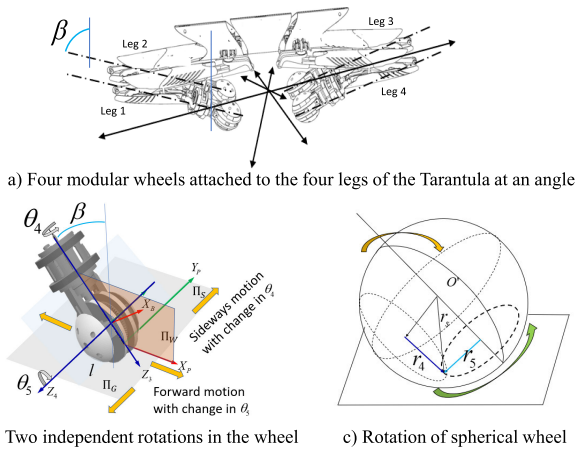
a) Four modular wheels attached to the four legs of the Tarantula at an angle

b) Two independent rotations in the wheel

c) Rotation of spherical wheel

FIGURE 22. Two independent rotation of the designed wheels for Tarantula-II.

FIGURE 23. The transformation gait sequence for the level shift of Tarantula-II.

length of the linear actuator in O_2PQR shown in Fig. 21 (b). Effectively each leg without considering the rotations in the wheel has three degrees of freedom. The kinematics of the leg is discussed next which is essential to know the height and required change in angle during the level shift process.

B. KINEMATICS OF THE WHEEL

The wheel to access the terrain of drainage system is designed. The omnidirectional locomotion along with the zero turning radius feature is desired while locomoting in the drain. Wheels with two independent rotations denoted by θ_4 and θ_5 are shown in Fig. 22 (b). The wheels are assembled at an angle β with the legs of the Tarantula-II as an end-effector. Fig. 22 (c) shows the two rotation which takes place and with variation in θ_2 the radius of rolling of the spherical wheel also changes. Due to the complexity of the geometry, the wheel radius r_3 that changes due to the change in steering angle is estimated assuming it as continuous sphere gives:

$$r_4(\beta, \theta_3) = r_s\sqrt{\sin^2\theta_3\cos^2(\beta) + \cos^2(\theta_3)} \quad (6)$$

Also the effective steering rolling radius r_5 can be easily calculated using Fig. 22 (c) as:

$$r_5(\beta) = r_s\sin(\beta) \quad (7)$$

The above two equations governs the rotation of the wheel which is mounted at an angle β to each of the leg. The details of kinematics of wheel is reported in another work.

C. GAIT FOR THE LEVEL SHIFT

Level-shifting capability of the Tarantula-II platform, is achieved by using IR sensor and inertial measuring unit (IMU). The IR sensors are placed at two position behind the hip joints to get the depth of the drain. An IMU sensor is provided to monitor the pitch angle of the trunk body and follow a PID controller to keep the trunk body horizontally through out the level shifting. The extension of both forelegs and hind legs follow the inverse kinematics equations. The platform
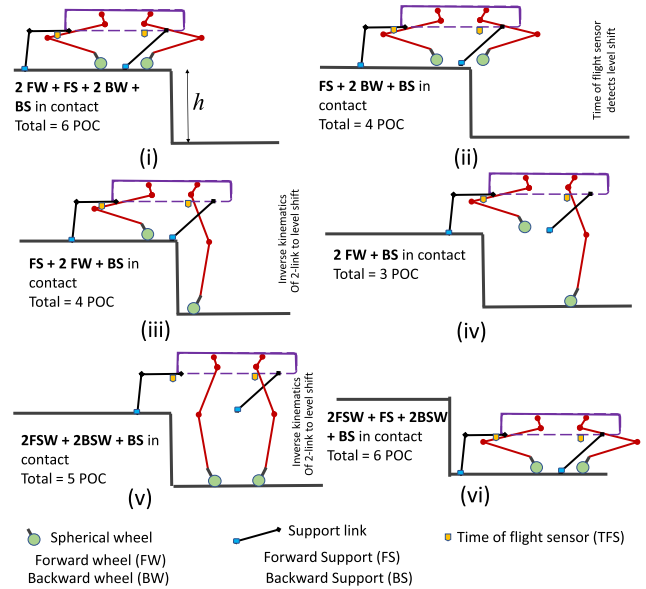
follows the stability algorithm as mentioned in Fig. 8. In this section, we describe the execution process of the gaits of each leg during level changes. The following steps were followed during climbing down across a level.

- The platform was deployed on flat ground with retracted legs with the platform at its lowest height.
- The IR sensor mounted on the platform measure the depth of the drain and send command to the motion controller.
- By using the inverse kinematics equation, the motion controller, regulates the angular rotation of each joint of the forelegs as per the depth data given by time of flight sensor.
- The platform keeps the extended fore legs and tail mechanism with auxiliary wheels inside the drain and the controller also corrects the posture of the trunk body (maintaining the horizontal position).
- Then, the platform gradually moves forward and the hind legs undergo extension and crosses the level.

Figure 23 shows the gait sequence for the level shift of Tarantula-II. Note that the addition support wheels ensures the four point of contact of the platform at a given time during the level shift.

D. FORWARD AND INVERSE KINEMATICS OF LEG

The trunk body of the platform is supported on four wheeled-leg assemblies. As the legs are of the same structure, it is sufficient to investigate the kinematics analysis of single leg. Figure 24 shows the coordinate frame and the angular rotation of each joint of the right foreleg. Each leg and wheel has three and two degrees of freedom, respectively. The center of the rolling wheel is considered as the end-effector. Each leg consists of three links and the joints are numbered from 1 to 4 as shown in Fig. 24. Let link length l_i, link twist α_i,

(a)

Link	Link Length l_i	Link Twist α_i	Joint Offset d_i	Joint angle θ_i
1	0	90	d_1	θ_1
2	l_2	0	0	θ_2
3	l_3	0	0	θ_3

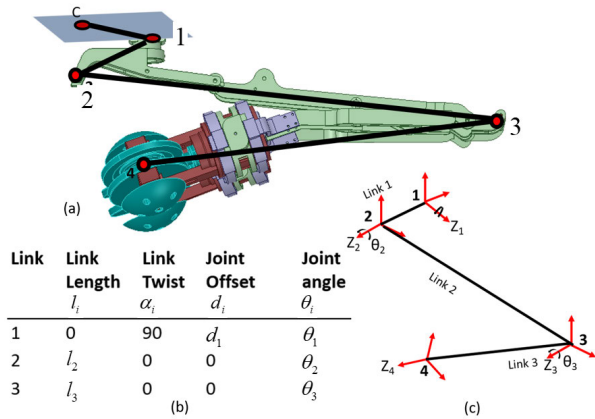(b)   (c)

FIGURE 24. Schematic diagram of a leg showing the coordinate frames at each joint and Denavit–Hartenberg parameters.

a) Workspace of two links with varying θ_2 and θ_3

b) All the three joints actuated in a range with the hip joints θ_1 rotated by 90 degrees

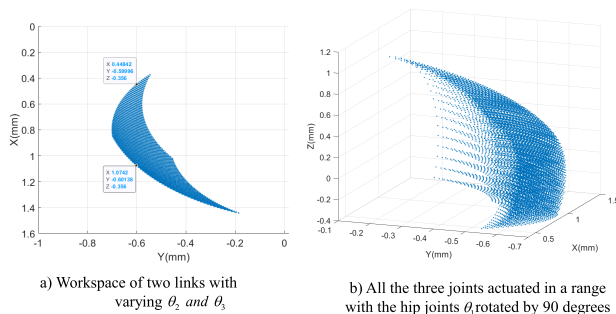**FIGURE 25.** Workspace of the Tarantula-II leg with the limited actuation as $0 < \theta_2 < 50$, $35 < \theta_3 < 75$ and the hip joint θ_1 from 0 to 90 degrees.

joint distance d_i, and joint angle θ_i are the Denavit-Hartenberg parameters of ith joint, where $i = 1, 2,$ and 3. The joint 1 is a revolute joint, which rotates the whole leg about the Z_1 axis. The joint 2 and 3 are also revolute joints and move about Z_2 and Z_3 axis, respectively, in a plane perpendicular to the axis of joint 1. The joint 4 is the center of the rolling unit of the wheel. Let θ_1, θ_2, and θ_3 are joint angle at the joint 1, joint 2 and joint 3, respectively. The homogeneous transformation matrix (HTM) describing the translation and rotation between the successive joints are given Equations (15)-(17). The transformation matrix that describes from the hip joint frame to wheel center is ${}^0\mathbf{T}_3 = {}^0\mathbf{T}_1 {}^1\mathbf{T}_2 {}^2\mathbf{T}_3$, described by Equation (18) in Appendix A. The workspace of of one of the leg is plotted in two dimensional plane as in Fig. 25 (a) which is also the front view of the leg moved by actuating θ_2 and θ_3 in a limit. The rotation of the hip joint will result in the three dimensional workspace of each leg as shown in Fig. 25 (b). Note that the point of center of the wheel is taken as end effector and the link length for the femur and tibia is $l_2 = 0.310$ and $l_3 = 0.65$ meters. These leg lengths were estimated using the circle point method reported in [31] and for Tarantula-I in [27].

The inverse kinematic solution of the Tarantula-II robot, is performed to estimate the joint variables, given the position of the wheel center. Denoting the coordinates of the
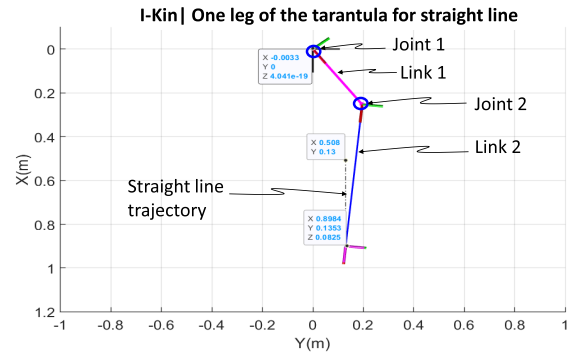
a) Leg of tarantula performing straight line motion during level shift
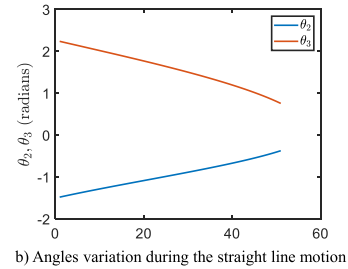
b) Angles variation during the straight line motion

FIGURE 26. Inverse kinematic of two link participating during the level shift of the leg.

wheel center by $[x, y, z]^T$ and equating the respective position component from the composite transformation matrix ${}^0\mathbf{T}_3$, as described in Appendix. We get Equations (8-10), where, $(S_{23} = \sin(\theta_2 + \theta_3), C_{23} = \cos(\theta_2 + \theta_3))$. The position of the wheel center is only a function of the joint angles θ_1, θ_2, and θ_3. By solving, Equations (8)-(10) analytically, the closed form solutions are obtained, given by Equations (11)-(13),

$$x = C_1(l_2C_2 + l_3C_{23}) \tag{8}$$

$$y = S_1(l_2C_2 + l_3C_{23}) \tag{9}$$

$$z = d_1 + l_2S_2 + l_3C_{23} \tag{10}$$

$$\theta_1 = \tan^{-1}\left(\frac{x}{y}\right) \tag{11}$$

$$\theta_2 = \sin^{-1}(z - d_1) - \alpha \tag{12}$$

$$\theta_3 = \cos^{-1}\frac{(x^2 + y^2 + (z - d_1)^2 - a_2^2 - a_3^2)}{2a_2a_3} \tag{13}$$

where, $\alpha = \tan^{-1}\frac{a_3\sqrt{1-A^2}}{a_2+a_3A}$, and $A = \frac{x^2+y^2+(z-d_1)^2-a_2^2-a_3^2}{2a_2a_3}$

Note that the above derivation is used to estimate the angular position of the two joints, i.e., θ_1 and θ_2 while the level shift action is performed as mentioned in Section V-C. Once the two wheels is in open air the height of the level shift is sensed by the time of flight sensor or IR sensor and the inverse kinematics routine calculates the angular variation of the two joints. The initial coordinate is assumed as $(0, 0)$ and the height sensed by IR sensor (say h) is used as the final coordinates to be reached by the point O_4. The joint angles were calculated for the end-effector to move from initial position to final position as shown in Fig. 26 (a) and the angles as shown Fig. 26 (b) were subsequently used to find the length of linear actuators governed by Equation (5).
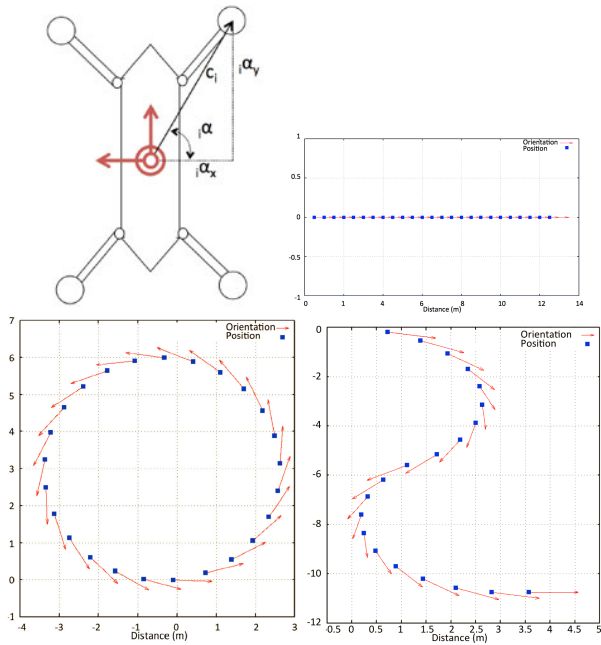
FIGURE 27. Simulated trajectories of the platform.

FIGURE 28. Angle of rotation of (a) the hip-femur and (b) femur-tibia joints of each leg.

E. PLATFORM'S KINEMATICS MODELING

Tarantula-II being a wheel robot, can modify the point of contact of its extremities on the ground. This is very useful during the movement of the robot along the drainage path. Since the drain channels have a different width, the robot must adapt to the different dimensions to perform correct navigation. By varying the contact points of the extremities with the ground, the interaction of the wheels with the ground and the contribution to the displacement are affected. Thus, it is necessary to know the contribution of each leg in robot's locomotion. Let v_i, α_i, and c_i are the translational velocities of ith wheel, the orientation of the ith wheel from the center of the platform, and radial distance of the ith wheel from the center of the platform, respectively ($i = 1$ to 4). The platform's linear velocity (v_p) and angular velocity (ω_p) is given by the Equation (14). Symbol c_i denotes the distance from the inertial system of the robot to the point of contact in the ground using the kinematic equation of the leg p_i and the distance to the assembling point $[x_e, y_e]^\top$, where $c_i = \sqrt{x_i^2 + y_i^2} + \|\mathbf{p}\|$. These kinematics equations are used to simulate the locomotion of the platform on three different trajectories including straight line, circular, and 'S' profile, as shown in Fig. 27.

$$v_p = \frac{\sum_{i=1}^{n} v_i}{4}$$

$$\omega_p = \frac{(v_1 + v_2 - v_3 - v_4)\cos(\alpha_1 + \alpha_2 + \alpha_3 + \alpha_4)}{c_1 + c_2 + c_3 + c_4} \quad (14)$$

VI. DESIGN VALIDATION AND DISCUSSIONS

This section demonstrate the capabilities of the designed robot in the drain environment.
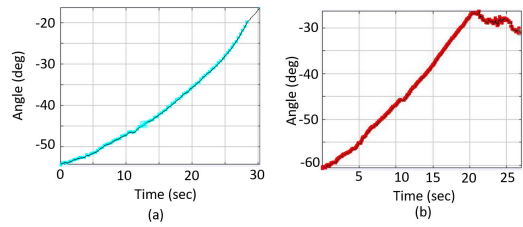
A. RECONFIGURATION ABILITY

The angular positions of the giraffe joints, inspire the legs orientation and leg folding pattern for the robotic platform, obtaining the following postural results in Tarantula-II. The angular rotation of the both joints were measured by tracking video. Figure 28 presents the real time angle of rotation of hip-femur (upper) and femur-tibia (lower) joint. By varying the angular rotation of the joints driven by the linear actuators, the platform is able to attend the maximum and minimum height as 50 cm and 110 cm, respectively. During setting, both legs are folded outwards such that the centre of gravity always lies inside the trunk's body.

B. LOCOMOTION CAPABILITY

In this section, we validate the locomotion capability, level-shifting, reconfiguration ability, of the platform by operating the robot in lab and drain setting. The locomotion ability of the Tarantula-II platform was verified in lab setting by adapting the following procedure. By adjusting the linear actuators and abduction motor, the heights of all the four legs are made equal. The feed back from inertial measuring unit was noted to ensure the zero tilt of the trunk body. A camera was mounted on the ceiling to capture the video of the platform's locomotion. We observed that the platform is able to move forward, backward, side wise, and also follow a circular path smoothly in lab setting as the floor is smooth. By rotating all the wheels clockwise and anticlockwise about the rolling axis, the platform is able to move forward or backward, respective, shown in Fig. 29 (a). By the rotating the wheel about steering axis clockwise and anticlockwise, the platform is able to move side wise, as shown in Fig. 29 (b). By maintaining a velocities difference among the left and right side wheels, the platform is able to achieve locomotion along a curved path, shown in Fig. 29 (c).

C. LEVEL-SHIFTING CAPABILITY

The level change capability of Tarantula-II, was verified on a wooden block. The following steps were followed during climbing down the wooden platform. First, the robot's was deployed on flat ground with its legs at its lowest height, shown in Fig. 30 (a). By using the Graphical User Interface (GUI) of the PC, the joint rotation of each leg joint was controlled to have the full extended position. Then, the platform with extended hind legs kept the fully bent forelegs on the wooden block and gradually climbed up. During this
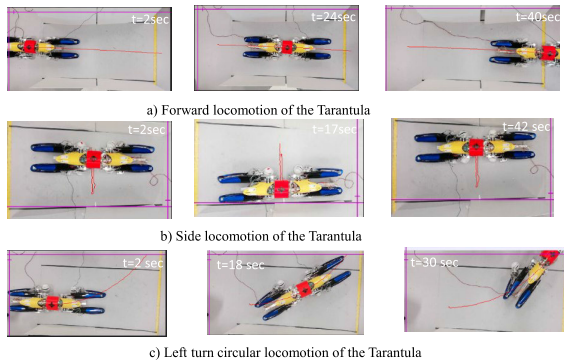
a) Forward locomotion of the Tarantula

b) Side locomotion of the Tarantula

c) Left turn circular locomotion of the Tarantula

FIGURE 29. Platform undergoes (a) forward movement (b) side-wise movement, and (c) left turn in lab setting.

(a) Level shift gait in the lab settings with step height of 0.65 meters

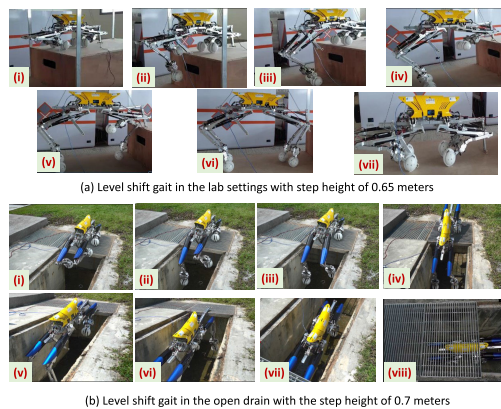(b) Level shift gait in the open drain with the step height of 0.7 meters

FIGURE 30. (a) Level shifting in lab setting and (b)locomotion and level-shifting in drain environment.
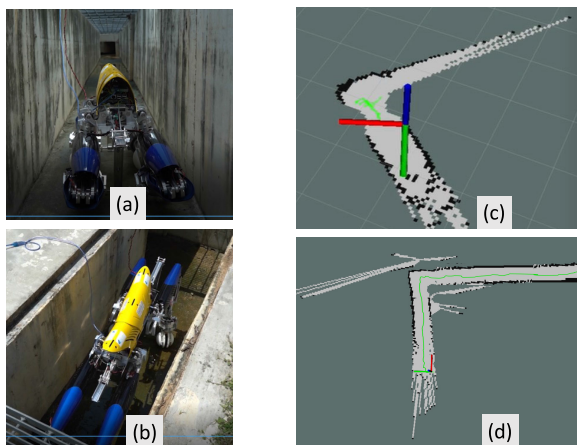

FIGURE 31. Platform with LiDAR mounted moves inside the drain.

level transitioning, the IMU sensor, connected to the trunk body, does the posture correction of the robot. The pitch angle is monitored from the IMU sensor and is later fed to the controller. The error signal from the controller operates on the posture of the trunk body and upon optimizing the error the slave PC actuates the necessary actuators to maintain the stability of the robot by making the pitch angle lie between the

threshold limits. The pitch angle is continuously monitored to keep it under the threshold limits. Figure 30 (a) shows various pose with the trunk maintaining horizontal position.

D. DEPLOYMENT IN DRAIN ENVIRONMENT

Tarantula-II platform was deployed in the drain with a level shift of 70 cm and width 80 cm. Figure 30 (b) shows the level shifting and locomotion capability of the platform in the drain. The platform takes around three minutes to cross the level. We observed that, the platform undergoes with a slight deviation from the straight path. This deviation is mainly due to rough surface that provides friction to slow down the motion. A 2D LiDAR was mounted on the anterior side of the platform to capture the map of the drain. Figure 31 shows the 2D map of a L-shaped drain environment.

VII. CONCLUSION

In this paper, mechanical design and software architecture of a bio-inspired drain mapping robot, Tarantula-II is presented. The postures of this platform are based on the fact that the giraffe, being a high-altitude animal, can maintain balance through the articulation of its legs. Observing the postural comparisons previously shown, we can say that the adaptation of the giraffe to change its height applied to Tarantula-II has advantages over other types of locomotion: since it gives the facility to realize sudden changes of level as they are steps. In the same way, it helps displacement in unstructured terrains with steep slopes that can be very complex for rolling robots. From the mechanical model of the platform, forward and inverse kinematics models were discussed. Based on the the DH parameters of each leg, the workspace of the wheel center was studied. It was found that the geometry of the mechanism, the distance between the position of the center of the trunk body and the wheel center of each leg imposes a constraint. We also validated the kinematics principle and verified the forward, backward, side wise and rotational movement capability of the of the platform. The reconfiguration ability of the platform during level shifting in lab setting and the actual environment was monitored. We observed that platform takes about three minute to climbing down the level of 70 cm.

The environmental conditions in the real drain environment pose a challenge while adapting on wet surface and with obstacles along the path. The future research work aims at increasing the autonomy level index [28] which has to be achieved by focusing on the weight optimization, locomotion ability of platform on various rough terrain, stability analysis, wall collision avoidance, controller design for the leg joints.

APPENDIX A
A: FORWARD KINEMATICS ANALYSIS

The transformation matrix of leg from the hip joint attached to the body to the point on the wheel consist of the three joints.

The forward kinematics of each leg is represented as below:

$$
{}^0T_1 = \begin{bmatrix} C_1 & 0 & S_1 & 0 \\ S_1 & 0 & -C_1 & 0 \\ 0 & 1 & 0 & d_1 \\ 0 & 0 & 0 & 1 \end{bmatrix} \tag{15}
$$

$$
{}^1T_2 = \begin{bmatrix} C_2 & -S_2 & 0 & l_2C_2 \\ S_2 & C_2 & 0 & l_2S_2 \\ 0 & 0 & 1 & 0 \\ 0 & 0 & 0 & 1 \end{bmatrix} \tag{16}
$$

$$
{}^2T_3 = \begin{bmatrix} C_3 & -S_3 & 0 & l_3C_3 \\ S_3 & C_3 & 0 & l_3S_3 \\ 0 & 0 & 1 & 0 \\ 0 & 0 & 0 & 1 \end{bmatrix} \tag{17}
$$

$$
{}^0T_3 = {}^0T_1 {}^1T_2 {}^2T_3 = \begin{bmatrix} r_{11} & r_{12} & r_{13} & r_{14} \\ r_{21} & r_{22} & r_{23} & r_{24} \\ r_{31} & r_{32} & r_{33} & r_{34} \\ r_{21} & r_{42} & r_{43} & r_{44} \end{bmatrix} \tag{18}
$$

where,

$r_{11} = C_1C_2C_3 - C_1S_2S_3,$

$r_{12} = -C_1C_2S_3 - C_1S_2C_3,$

$r_{13} = S_1,$

$r_{14} = l_2C_1C_2 + l_3C_1C_2C_3 - l_3C_1S_2C_3,$

$r_{21} = C_2C_3S_1 - S_1S_2S_3,$

$r_{22} = -S_1C_2S_3 - S_1S_2C_3,$

$r_{23} = -C_1,$

$r_{24} = l_2S_1C_2 + l_3S_1C_2C_3 - l_3S_1S_2S_3,$

$r_{31} = C_2S_3 + C_3S_2,$

$r_{34} = d_1 + l_2S_2 + l_3C_2S_3 + l_3S_2C_3,$

$r_{32} = 0, r_{33} = 0, \quad r_{41} = 0, \ r_{42} = 0; \ r_{43} = 0; \ r_{44} = 1;$

REFERENCES

[1] R. Mosher, "Test and evaluation of a versatile walking truck," in *Proc. Off-Road Mobility Res. Symp.*, Washington, DC, USA, 1968, pp. 359–379.

[2] R. B. McGhee, "Some finite state aspects of legged locomotion," *Math. Biosci.*, vol. 2, nos. 1–2, pp. 67–84, Jan. 1968.

[3] S. Hirose, "A study of design and control of a quadruped walking vehicle," *Int. J. Robot. Res.*, vol. 3, no. 2, pp. 113–133, Jun. 1984.

[4] S. Hirose and K. Kato, "Study on quadruped walking robot in tokyo institute of technology-past, present and future," in *Proc. ICRA. Millennium Conf. IEEE Int. Conf. Robot. Automat. Symp.*, vol. 1, Apr. 2000, pp. 414–419.

[5] K. Arikawa and S. Hirose, "Development of quadruped walking robot TITAN-VIII," in *Proc. IEEE/RSJ Int. Conf. Intell. Robots Syst. (IROS)*, vol. 1, Nov. 1996, pp. 208–214.

[6] S. Kitano, S. Hirose, G. Endo, and E. F. Fukushima, "Development of lightweight sprawling-type quadruped robot TITAN-XIII and its dynamic walking," in *Proc. IEEE/RSJ Int. Conf. Intell. Robots Syst.*, Nov. 2013, pp. 6025–6030.

[7] K. Berns, W. Ilg, M. Deck, J. Albiez, and R. Dillmann, "Mechanical construction and computer architecture of the four-legged walking machine BISAM," *IEEE/ASME Trans. Mechatronics*, vol. 4, no. 1, pp. 32–38, Mar. 1999.

[8] T. Yanagida, R. Elara Mohan, T. Pathmakumar, K. Elangovan, and M. Iwase, "Design and implementation of a shape shifting rolling-crawling-wall-climbing robot," *Appl. Sci.*, vol. 7, no. 4, p. 342, Mar. 2017.

[9] I. Juárez-Campos, D. A. Núñez-Altamirano, L. Márquez-Pérez, L. Romero-Muñoz, M. E. Juárez-Campos, and B. Juárez-Campos, "Bioinspired sprawling robotic leg and a path-planning procedure," *Int. J. Adv. Robotic Syst.*, vol. 15, no. 1, 2018, Art. no. 1729881418759888.

[10] C. Wang, T. Zhang, X. Wei, Y. Long, and S. Wang, "Bio-inspired control strategy study for the quadruped robot with a segmented spine," *Ind. Robot, Int. J.*, vol. 44, no. 1, pp. 85–93, Jan. 2017.

[11] V. Krovi and V. Kumar, "Modeling and control of a hybrid locomotion system," 1999.

[12] G. Muscato and G. Nunnari, "Leg or wheels? WHEELEG a hybrid solution," in *Proc. Int. Conf. Climbing Walking Robots (CLAWAR)*, 1999.

[13] M. Guihard, P. Gorce, and J. G. Fontaine, "SAPPHYR: Legs to pull a wheel structure," in *Proc. IEEE Int. Conf. Syst., Man Cybern. Intell. Syst. 21st Century*, vol. 2, Oct. 1995, pp. 1303–1308.

[14] Y. Ichikawa, N. Ozaki, and K. Sadakane, "A hybrid locomotion vehicle for nuclear power plants," *IEEE Trans. Syst., Man, Cybern.*, vol. SMC-13, no. 6, pp. 1089–1093, Nov. 1983.

[15] A. Halme, I. Leppänen, and S. Salmi, "Development of workpartner-robot–design of actuating and motion control system," in *Proc. 2nd Int. Conf. Climbing Walking Robots*, Portsmouth, U.K., 1999, pp. 657–666.

[16] Y.-J. Dai, E. Nakano, T. Takahashi, and H. Ookubo, "Motion control of leg-wheel robot for an unexplored outdoor environment," in *Proc. IEEE/RSJ Int. Conf. Intell. Robots Syst. (IROS)*, vol. 2, Nov. 1996, pp. 402–409.

[17] K. Suwannasit and S. Laksanacharoen, "A bio-inspired hybrid leg-wheel robot," in *Proc. IEEE Region 10 Conf. (TENCON)*, vol. 500, Nov. 2004, pp. 495–497.

[18] R. Kirkham, P. D. Kearney, K. J. Rogers, and J. Mashford, "PIRAT—A system for quantitative sewer pipe assessment," *Int. J. Robot. Res.*, vol. 19, no. 11, pp. 1033–1053, 2000.

[19] H. B. Kuntze, D. Schmidt, H. Haffner, and M. Loh, "KARO—A flexible robot for smart sensor-based sewer inspection," in *Proc. Int. Conf. Dig.*, Dresden, Germany, 1995, pp. 367–374.

[20] R. Bradbeer, K. K. Ku, L. F. Yeung, and K. Y. Lam, "An underwater camera for security and recreational use," in *Proc. 9th Int. Symp. Consum. Electron. (ISCE)*, 2005, pp. 364–368.

[21] F. Kirchner and J. Hertzberg, "A prototype study of an autonomous robot platform for sewerage system maintenance," *Auto. Robots*, vol. 4, no. 4, pp. 319–331, 1997.

[22] E. Rome, J. Hertzberg, F. Kirchner, U. Licht, and T. Christaller, "Towards autonomous sewer robots: The MAKRO project," *Urban Water*, vol. 1, no. 1, pp. 57–70, Mar. 1999.

[23] A. A. F. Nassiraei, Y. Kawamura, A. Ahrary, Y. Mikuriya, and K. Ishii, "Concept and design of a fully autonomous sewer pipe inspection mobile robot 'KANTARO,'" in *Proc. IEEE Int. Conf. Robot. Autom.*, Apr. 2007, pp. 136–143.

[24] G. Granosik, "Hypermobile robots-the survey," *J. Intell. Robotic Syst.*, vol. 75, no. 1, pp. 147–169, Jul. 2014.

[25] A. Baghani, M. N. Ahmadabadi, and A. Harati, "Kinematics modeling of a wheel-based pole climbing robot (UT-PCR)," in *Proc. IEEE Int. Conf. Robot. Autom.*, Apr. 2005, pp. 2099–2104.

[26] P. R. Ratanghayra, A. A. Hayat, and S. K. Saha, "Design and analysis of spring-based rope climbing robot," in *Machines, Mechanism and Robotics*. Singapore: Springer, 2019, pp. 453–462.

[27] A. A. Hayat, K. Elangovan, M. Rajesh Elara, and M. S. Teja, "Tarantula: Design, modeling, and kinematic identification of a quadruped wheeled robot," *Appl. Sci.*, vol. 9, no. 1, p. 94, Dec. 2018.

[28] N. Tan, A. A. Hayat, M. R. Elara, and K. L. Wood, "A framework for taxonomy and evaluation of self-reconfigurable robotic systems," *IEEE Access*, vol. 8, pp. 13969–13986, 2020.

[29] [Online]. Available: https://www.youtube.com/watch?v=jE_Hb_1QsfU

[30] E. Williams, "Giraffe stature and neck elongation: Vigilance as an evolutionary mechanism," *Biology*, vol. 5, no. 3, p. 35, Sep. 2016.

[31] A. A. Hayat, R. A. Boby, and S. K. Saha, "A geometric approach for kinematic identification of an industrial robot using a monocular camera," *Robot. Comput.-Integr. Manuf.*, vol. 57, pp. 329–346, Jun. 2019.

RIZUWANA PARWEEN (Member, IEEE) received the bachelor's and master's degrees in mechanical engineering from the National Institute of Technology Rourkela, India, and the Ph.D. degree from the Indian Institute of Science, Bengaluru, India. She is currently a Research Fellow with the Engineering Product Development Pillar, Singapore University of Technology and Design (SUTD). She has over two years of industrial experience as a Product Development Engineer (KSB Tech Private Ltd., Pune, India) and Structural Analyst (CUMMINS, Pune). As a Postdoctoral Research Fellow with SUTD, she has worked on the design and development of Unloader Knee Brace for Asian Patients, in collaboration with physicians in Changi General Hospital, Singapore. As a Research Fellow, she is currently working on the design, development, and modeling of the self-reconfigurable floor cleaning robots.

ABDULLAH AAMIR HAYAT received the Bachelor of Technology degree in mechanical engineering from the Zakir Hussain College of Engineering and Technology (ZHCET), AMU, Aligarh, in 2009, the Master of Technology degree, in 2011, and the Ph.D. degree from IIT Delhi, India. He has worked as a Junior Research Fellow (JRF) with the Programme for Autonomous Robotics (PAR) Laboratory. He has been a Postdoctoral Research Fellow with the Singapore University of Technology and Design, Singapore, since May 2018. His research interests include Kinematic identification, calibration, multi-body dynamics, and reconfigurable robotics.

KARTHIKEYAN ELANGOVAN received the B.E. degree from Annamalai University, India, the M.Sc. degree in information technology from Sikkim Manipal University, India, and the Ph.D. degree in advanced multidisciplinary engineering from Tokyo Denki University, Japan. He is currently a Research Fellow with the Singapore University of Technology and Design (SUTD). Before joining SUTD, he was a Production Engineer in International Automotive components, India. His research interests include robotics with an emphasis on self-reconfigurable platforms. He was a recipient of the SG Mark Design Award, in 2017 and 2018, and the Design Award, in 2018.

KOPPAKA GANESH SAI APUROOP received the bachelor's degree from Amrita University, India, with majors in electronics and communication engineering discipline, in 2018. He is currently pursuing the master's degree under the SUTD-CGU Dual Masters Programme (Singapore-Taiwan). His research interests include artificial intelligence for robots, path planning in autonomous robots, and embedded systems.

MANUEL VEGA HEREDIA received the degree in electromechanical engineering, the master's degree in industrial engineering, and the Ph.D. degree in engineering sciences, with a specialization in robotics, from the Autonomous University of Ciudad Juarez, Mexico, in 2016. He was a Postdoctoral Research Fellow with the Singapore University of Technology and Design, from 2018 to 2020. He is currently a full-time Professor with the Universidad Autonoma de Occidente.
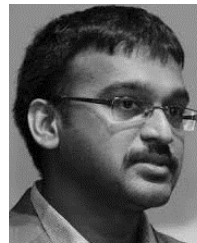
MOHAN RAJESH ELARA received the B.E. degree from the Amrita Institute of Technology and Sciences, Bharathiar University, India, and the M.Sc. degree in consumer electronics and the Ph.D. degree in electrical and electronics engineering from Nanyang Technological University, Singapore. He is currently an Assistant Professor with the Engineering Product Development Pillar, Singapore University of Technology and Design (SUTD). Before joining SUTD, he was a Lecturer with the School of Electrical and Electronics Engineering, Singapore Polytechnic. He is also a Visiting Faculty Member of the International Design Institute at Zhejiang University, China. He has published more than 80 articles in leading journals, books, and conferences. His research interests include robotics with an emphasis on self-reconfigurable platforms as well as research problems related to robot ergonomics and autonomous systems. He was a recipient of the SG Mark Design Award, in 2016, 2017, and 2018, the Design Award, in 2018, the ASEE Best of Design in Engineering Award, in 2012, and the Tan Kah Kee Young Inventors Award, in 2010. He has served in various positions of organizing and technical committees of over 20 international competitions and conferences.

• • •